Improving thin-film crystalline silicon solar cell efficiencies with photonic crystals

Peter Bermel,[1*] Chiyan Luo,[1] Lirong Zeng,[2] Lionel C. Kimerling,[2] and John D. Joannopoulos[1]

1 Center for Materials Science and Engineering Massachusetts Institute of Technology, Cambridge, MA 02139, USA

2 Department of Materials Science and Engineering, Massachusetts Institute of Technology, Cambridge, MA 02139, USA

bermel@mit.edu

Abstract: Most photovoltaic (solar) cells are made from crystalline silicon (c-Si), which has an indirect band gap. This gives rise to weak absorption of one-third of usable solar photons. Therefore, improved light trapping schemes are needed, particularly for c-Si thin film solar cells. Here, a photonic crystal-based light-trapping approach is analyzed and compared to previous approaches. For a solar cell made of a 2 μm thin film of c-Si and a 6 bilayer distributed Bragg reflector (DBR) in the back, power generation can be enhanced by a relative amount of 24.0% by adding a 1D grating, 26.3% by replacing the DBR with a six-period triangular photonic crystal made of air holes in silicon, 31.3% by a DBR plus 2D grating, and 26.5% by replacing it with an eight-period inverse opal photonic crystal.

OCIS codes: (230.5298) Photonic crystals; (350.6050) Solar energy.

References and links

1. C. Herzinger, B. Johs, W. McGahan, J. Woollam, and W. Paulson, "Ellipsometric determination of optical constants for silicon and thermally grown silicon dioxide via a multi-sample, multi-wavelength, multi-angle investigation," J. Appl. Phys. **83**, 3323–3336 (1998).
2. ASTMG173-03, *Standard Tables for Reference Solar Spectral Irradiances: Direct Normal and Hemispherical on 37 degree Tilted Surface* (ASTM International, West Conshohocken, Pennsylvania, 2005).
3. A. Rohatgi, E. Weber, and L. C. Kimerling, "Opportunities in silicon photovoltaics and defect control in photovoltaic materials," J. Electron. Mater. **22**, 65–72 (1993).
4. D. Fischer, S. Dubail, J. Selvan, N. P. Vaucher, R. Platz, C. Hof, U. Kroll, J. Meier, P. Torres, H. Keppner, N. Wyrsch, M. Goetz, A. Shah, and K.-D. Ufert, "The micromorph solar cell: extending a-Si:H technology towards thin film crystalline silicon," Twenty-fifth Photovolt. Spec. Conf. p. 1053 (1996).
5. R. Brendel, *Thin-Film Crystalline Silicon Solar Cells* (Wiley-VCH, Weinheim, Germany, 2003).
6. K. Wada, L. C. Kimerling, and N. Toyoda, "Back reflector of solar cells," (June 15, 2004). US patent no. 6750393.
7. E. Yablonovitch and G. Cody, "Intensity enhancement in textured optical sheets for solar cells," IEEE Trans. Electron Devices **ED-29**, 300–305 (1982).
8. R. Brendel, M. Hirsch, R. Plieninger, and J. Werner, "Quantum efficiency analysis of thin-layer silicon solar cells with back surface fields and optical confinement," IEEE Trans. Electron Devices **43**, 1104–1113 (1996).
9. P. Campbell and M. A. Green, "Light trapping properties of pyramidally textured surfaces," J. Appl. Phys. **62**, 243–249 (1987).
10. L. Feitknecht, J. Steinhauser, R. Schluchter, S. Fay, D. Domine, E. Vallat-Sauvin, F. Meillaud, C. Ballif, and A. Shah, "Investigations on fill-factor drop of microcrystalline silicon p-i-n solar cells deposited onto highly surface-textured ZnO substrates," in *Tech. Digest PVSEC-15* (Shanghai, China, 2005).

11. H. Bender, J. Szlufcik, H. Nussbaumer, G. Palmers, O. Evrard, J. Nijs, R. Mertens, E. Bucher, and G. Willeke, "Polycrystalline silicon solar cells with a mechanically formed texturization," Appl. Phys. Lett. **62**, 2941–2943 (1993).

12. J. Gee, "Optically enhanced absorption in thin silicon layers using photonic crystals," in *Twenty-Ninth IEEE Photovolt. Spec. Conf.*, pp. 150–153 (2002).

13. L. Zeng, Y. Yi, C.-Y. Hong, X. Duan, and L. C. Kimerling, "New Light Trapping in Thin Film Solar Cells Using Textured Photonic Crystals," in *Mater. Res. Soc. Symp. Proc.*, vol. 862 (Materials Research Society, Boston, MA, 2005).

14. L. Zeng, P. Bermel, Y. Yi, N. Feng, C.-Y. Hong, X. Duan, J. D. Joannopoulos, and L. C. Kimerling, "Optimization of textured photonic crystal backside reflectors for silicon thin-film solar cells," in *Mater. Res. Soc. Symp. Proc.*, vol. 974E (Materials Research Society, Boston, MA, 2006).

15. L. Zeng, Y. Yi, C.-Y. Hong, J. Liu, N. ning Feng, X. Duan, L. C. Kimerling, and B. Alamariu, "Efficiency enhancement in Si solar cells by textured photonic crystal back reflector," Appl. Phys. Lett. **89**, 111,111 (2006).

16. N.-N. Feng, J. Michel, L. Zeng, J. Liu, C.-Y. Hong, L. C. Kimerling, and X. Duan, "Design of Highly Efficient Light-Trapping Structures for Thin-Film Crystalline Silicon Solar Cells," IEEE Trans. Electron Devices **54**, 1926–1933 (2007).

17. S. Nishimura, N. Abrams, B. A. Lewis, L. I. Halaoui, T. E. Mallouk, K. D. Benkstein, J. van de Lagemaat, and A. J. Frank, "Standing Wave Enhancement of Red Absorbance and Photocurrent in Dye-Sensitized Titanium Dioxide Photoelectrodes Coupled to Photonic Crystals," J. Am. Chem. Soc. **125**, 6306–6310 (2003).

18. A. Mihi and H. Miguez, "Origin of Light-Harvesting Enhancement in Colloidal-Photonic-Crystal-Based Dye-Sensitized Solar Cells," J. Phys. Chem. B **109**, 15,968–15,976 (2005).

19. C. Huisman, J. Schoonman, and A. Goossens, "The application of inverse titania opals in nanostructured solar cells," Solar Energy Materials and Solar Cells **85**, 115–124 (2005).

20. S. Pillai, K. Catchpole, T. Trupke, G. Zhang, J. Zhao, and M. A. Green, "Enhanced emission from Si-based light-emitting diodes using surface plasmons," Appl. Phys. Lett. **88**, 161,102 (2006).

21. P. Sheng, A. Bloch, and R. Stepleman, "Wavelength-selective absorption enhancement in thin-film solar cells," Appl. Phys. Lett. **43**, 579–581 (1983).

22. R. H. Morf and H. Kiess, "Submicron gratings for light trapping in silicon solar cells: a theoretical study," in *Proc. Ninth Internat. Conf. Photovolt. Solar Energy*, W. Palz, ed., pp. 313–315 (Commission of the European Communities, Brussels, 1989).

23. H. Kiess and R. H. Morf, "Light trapping in solar cells and determination of the absorbed energy by calorimetry," Proc. SPIE **1149**, 124–129 (1989).

24. M. Gale, B. Curtis, H. Kiess, and R. H. Morf, "Design and fabrication of submicron grating structures for light trapping in silicon solar cells," Proc. SPIE **1272**, 60–66 (1990).

25. C. Heine and R. H. Morf, "Submicrometer gratings for solar energy applications," Appl. Opt. **34**, 2476–2482 (1995).

26. S. H. Zaidi, J. M. Gee, and D. S. Ruby, "Diifraction grating structures in solar cells," in *Twenty-Eighth IEEE Photovolt. Spec. Conf.*, pp. 395–398 (2000).

27. C. Eisele, C. Nebel, and M. Stutzmann, "Periodic light coupler gratings in amorphous thin film solar cells," J. Appl. Phys. **89**, 7722–7726 (2001).

28. S. H. Zaidi, R. Marquadt, B. Minhas, and J. Tringe, "Deeply etched grating structures for enhanced absorption in thin c-Si solar cells," in *Twenty-Ninth IEEE Photovolt. Spec. Conf.*, p. 1290 (2002).

29. F. Llopis and I. Tobias, "The role of rear surface in thin silicon solar cells," Sol. Energy Mater. Sol. Cells **87**, 481–492 (2005).

30. T. Ogawa and Y. Kanemitsu, eds., *Optical Properties of Low-Dimensional Materials* (World Scientific, Singapore, 1995).

31. J. Joannopoulos, R. Meade, and J. Winn, *Photonic Crystals: Molding the Flow of Light* (Princeton, Princeton, NJ, 1995).

32. N. W. Ashcroft and N. D. Mermin, *Solid State Physics* (Holt Saunders, Philadelphia, PA, 1976).

33. H. Kosaka, T. Kawashima, A. Tomita, M. Notomi, T. Tamamura, T. Sato, and S. Kawakami, "Superprism phenomena in photonic crystals," Phys. Rev. B **58**, R10,096–R10,099 (1998).

34. T. Tiedje, E. Yablonovitch, G. Cody, and B. Brooks, "Limiting efficiency of silicon solar cells," IEEE Trans. Electron Devices **31**, 711–716 (1984).

35. D. Whittaker and I. Culshaw, "Scattering-matrix treatment of patterned multilayer photonic structures," Phys. Rev. B **60**, 2610–2618 (1999).

36. K. S. Yee, "Numerical solution of inital boundary value problems involving maxwell's equations in isotropic media," IEEE Trans. Attennas Propag. **AP-14**, 302–307 (1966).

37. J. Berenger, "A perfectly matched layer for the absorption of electromagnetic waves," J. Comp. Phys. **114**, 185–200 (1994).

38. W. Shockley and H. J. Queisser, "Detailed balance limit of efficiency of p-n junction solar cells," J. Appl. Phys. **32**, 510 (1961).

39. C. Henry, "Limiting efficiencies of ideal single and multiple energy gap terrestrial solar cells," J. Appl. Phys. **51**,

4494–4500 (1980).

40. S. G. Johnson and J. D. Joannopoulos, "Block-iterative frequency-domain methods for Maxwell's equations in a planewave basis," Opt. Express **8**, 173–190 (2001).
41. J. Jackson, *Classical Electrodynamics* (Wiley, New York, 1999).
42. E. D. Palik, ed., *Handbook of Optical Constants of Solids*, vol. 1 (Academic Press, San Diego, CA, 1998).
43. S.-Y. Lin, J. Fleming, D. Hetherington, B. Smith, R. Biswas, K. Ho, M. Sigalas, W. Zubrzycki, S. Kurtz, and J. Bur, "A three-dimensional photonic crystal operating at infrared wavelengths," Nature **394**, 251–253 (1998).
44. Y. A. Vlasov, X.-Z. Bo, J. C. Sturm, and D. J. Norris, "On-chip natural assembly of silicon photonic bandgap crystals," Nature **414**, 289–293 (2001).
45. S. Takahashi, M. Okano, M. Imada, and S. Noda, "Three-dimensional photonic crystals based on double-angled etching and wafer-fusion techniques," Appl. Phys. Lett. **89**, 123,106 (2006).

1. Introduction

One of the foremost challenges in designing silicon photovoltaic cells is devising an efficient light-trapping scheme. Crystalline silicon (c-Si) have an indirect band gap, which gives rise to weak absorption of light in the near infrared (near-IR), with an absorption length that increases from just over 10 μm for $\lambda =$800 nm to over 1 mm for $\lambda =$1108 nm [1]. However, that range of wavelengths contains 36.2% of solar photons with energies above the band gap of c-Si [2]. Thus, solar cells made from c-Si thin films or 150 μm c-Si wafers will fail to absorb a significant number of photons that could otherwise be used to generate power in the cell. At the same time, the expense of thicker c-Si wafers, e.g., 775 μm, with their correspondingly longer diffusion lengths [3], drives up costs significantly. As a result, advanced light trapping schemes are needed in order to create thin yet efficient solar cells, made from c-Si and other, closely related materials, such as nanocrystalline silicon (which has the same bandgap and similar absorption characteristics [4]). There are two distinctive approaches to light trapping: geometrical optics, which is commonly used in solar cells today, and wave optics, which represents a new approach to the problem that has just begun to be explored.

Traditional approaches to light trapping in solar cells rely on controlling light ray paths through geometrical optics. Fig. 1(a) illustrates how these path lengths can be increased by two mechanisms: first, normally incident rays can be scattered into an angle at the front interface via surface texturing, and second, they can be reflected back into the cell via an aluminum reflector. Combining perfect random scattering at the front with a lossless reflector in the back theoretically enhances the effective path length by a factor of $4n^2$, corresponding to a value of about 50 for Si, and 30 for TiO$_2$ [7]. The performance of front surface texturing can be viewed in reference to the ideal Lambertian scatterer. It is designed to randomly scatter light into a uniform distribution of forward angles, known as a Lambertian distribution. However, no actual scattering surface is perfectly Lambertian in nature – the extent to which it replicates the ideal is typically called the "Lambertian fraction" Λ, and is typically 55% or less [8]. For example, the performance of a c-Si surface textured by etching (100)-oriented c-Si wafers with KOH to form (111)-oriented pyramids can be understood in these terms. Theoretically, in the best case of a random distribution of pyramids, the performance comes close to the ideal Lambertian scattering case [9]. However, it has been found that the fill factor (a measure of efficiency) is generally decreased by these surfaces [10, 11] – in the latter case, from 75% to 70%. This decrease is 6.7% in relative terms, which corresponds to the loss of a significant fraction of the gains associated with this light trapping technique. Furthermore, typical solar cells use aluminum on the back surface, which reflects no more than 80% of the light incident from the c-Si bulk region.

The light-trapping approach illustrated in this paper is based on wave optics, which has been shown to be capable, in principle, of outperforming all geometrical optics approaches (at least for a certain range of wavelengths) [5, 12]. This is because, in contrast to geometrical optics approaches that treat all wavelengths of light equally, wave optics approaches can be targeted
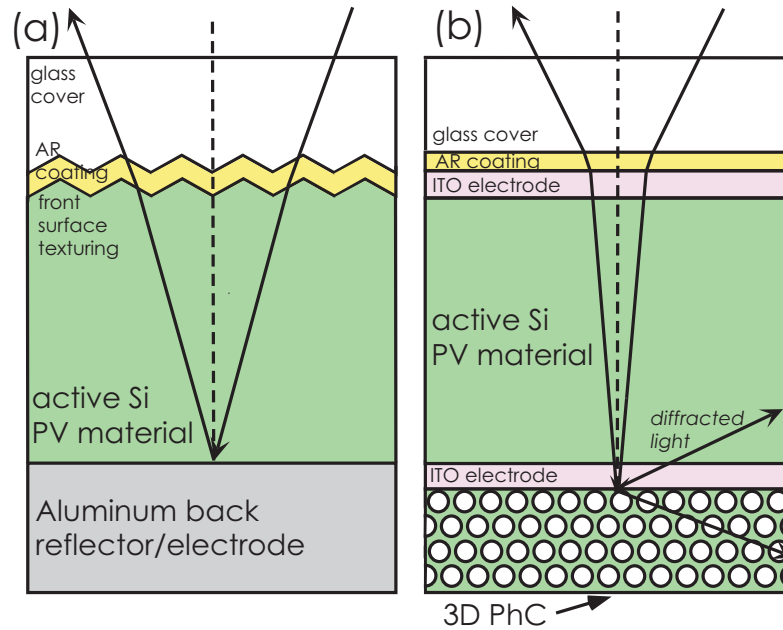
Fig. 1. (a) conventional solar cell design using traditional geometric optics concepts of reflection and refraction to trap light [5]; (b) novel solar cell design using wave optics (photonic crystals) to trap light with higher efficiency [6].

to enhance absorption only in the range where it can be most beneficial [5, 6, 12–16]. To date, there has been some work considering wave optics approaches to light-trapping. Several groups have considered using slow light in an inverse opal structure to enhance absorption of dye-sensitized photovoltaic cells [17–19]. One group has considered using surface-plasmon based coupling of light into cells via resonances at specific target wavelengths [20]. Some groups have used gratings to enhance the effective path length via diffraction [13–16, 21–29]. Past work on metal grating elements has shown that they can yield increased absorption, but not necessarily increased power generation efficiency [24]. On the other hand, dielectric gratings with planar metal back reflectors have shown overall efficiency improvements are possible [13–16, 26, 28]. In order to also limit the losses associated with metallic reflectors, some recent work has combined a distributed Bragg reflector (DBR) with a grating [13–16]. In this manuscript, three approaches to light trapping in solar cells are examined in detail: metallic gratings [21–25], dielectric gratings [13–16, 26–29], and 2D or 3D photonic crystals [6].

As illustrated in Fig. 1(b), there are three physical mechanisms by which wave optics approaches (based on DBRs, gratings, and photonic crystals) can improve light-trapping: reflection, diffraction, and refraction. First, these structures can offer reflection superior to highly absorptive aluminum reflectors [6, 13–16]. Distributed Bragg reflectors with high index contrast can reflect light over a broad range of incident angles and wavelengths, for either or both polarizations [30]. Similarly, a photonic crystal can reflect light incident from any angle for frequencies and polarizations within the photonic band gap [31]. Its origin is similar to that of the semiconductor band gap, to wit: in a periodic medium, waves must oscillate in a specific form, dictated by Bloch's theorem. When they vary with a period commensurate with the period of the crystal, they can concentrate their energy either in low or high dielectric, giving rise to two different allowed energies. The energies between form the photonic band gap, a range

of forbidden energies that are reflected at the surface. An additional advantage of the photonic crystal is that it can reflect light within the bandgap incident from any angle or medium, since the corresponding propagating modes are wholly forbidden. Second, wave optics-based devices can be designed to diffract incoming beams into highly oblique angles, according to Bragg's law [6, 13–16, 21–29, 32]. This applies both to gratings as well as photonic crystals, and in both cases, will depend primarily on the parameters of the device at the interface with homogeneous dielectric (e.g., the photovoltaic material). The diffraction induced by such an interface improves light trapping by increasing the distance that light must travel to return to the front surface of the cell. Furthermore, if the angle of the diffracted beam is greater than the critical angle, it will also be internally reflected back into the solar cell. In conjunction with a highly efficient reflector, a large number of bounces can be achieved. This effect is particularly significant for modes near the diffraction threshold. With the proper choice of grating periodicity, this effect can be targeted to the key near-IR region of the solar spectrum. Finally, there is an effect specific to a 2D or 3D photonic crystal made of the photovoltaic material: frequencies outside the photonic band gap can be refracted into modes with a high photon density of states in order to improve absorption efficiency [12]. Coupling can take place via a superprism-type effect [33]. Furthermore, even frequencies inside the photonic band gap can have their evanescent tails partially absorbed by the photonic crystal. All of these effects can be thought of as increasing the time spent by photons inside the solar cell, which helps to maximize the probability of absorption.

These wave optics-based approaches can be applied to thin-film solar cells, which offer the advantage of lower materials usage as well as lower bulk recombination losses and potentially higher open-circuit voltages [34]. These approaches are especially promising for thin film-based solar cells for two reasons. First, they are are not generally amendable to coarse texturing approaches that introduce features 5-10 μm in depth, while photonic crystals generally consist of several layers of thicknesses on the order of 300 nm. Second, thin films have the greatest potential to benefit from enhanced light trapping, since less light will be absorbed over a broader bandwidth than in wafer-based solar cells made of the same materials [6, 13–16].

2. Numerical methods

The light-trapping properties of the structures discussed in this paper are studied using a transfer matrix approach known as the S-matrix method [35]. The structure is broken up into slices with uniform symmetry in the z-direction, boundary conditions are imposed at one end, and fields are propagated throughout the structure. The boundary conditions employed in this work correspond to unpolarized light incident from directly above the solar cell. Light trapping is calculated by modeling the c-Si regions with a complex dielectric constant that depends on wavelength, as in Ref. 1. The c-Si region is treated as if it is only intrinsic, i.e., the doping of the $p-$ and $n-$doped regions can be considered to have a negligible impact on the optical properties of the device. In principle, this calculation of the model's optical properties is exact apart from discretization errors, which can be reduced systematically by increasing the resolution of the grid. Verification has been performed for several simulations using the finite-difference time domain method [36] with perfectly-matched boundary layers [37]. In general, the results are in good agreement, but the FDTD method is much slower for the same resolution, so it is not used for most calculations.

In order to calculate power generation efficiency from our model, we assume that each absorbed photon with energy greater than the band gap energy generates an electron-hole pair, and both carriers reach the electrical contacts. This corresponds to the statement that the diffusion length L_D is much greater than the distance traveled by each carrier (i.e., $L_D \gg d$). Power generation efficiency is given by $\eta = J[V(\max)]V(\max)/P_{\text{inc}} = (J_{sc}V_{OC}/P_{\text{inc}}) \times FF$, where P_{inc} is the

solar irradiance, $V(\max)$ and $J[V(\max)]$ are the voltage and current density at the maximum power point, respectively, the product of which equals the open-circuit voltage V_{oc} times the short-circuit current density J_{sc} times the fill factor FF. Following Refs. 38 and 39, the above quantities can be calculated as follows: first, the current density J as a function of the voltage V is given by the sum of the photon-induced current minus the intrinsic current generated by radiative recombination, i.e.,

$$J(V) = \int_0^\infty d\lambda \left[\frac{e\lambda}{hc} \frac{dI}{d\lambda} A(\lambda) \right] - \frac{e(n^2+1)E_g^2 kT}{4\pi^2 \hbar^3 c^2} \exp\left(\frac{eV - E_g}{kT} \right), \qquad (1)$$

where $\frac{dI}{d\lambda}$ represents the light intensity experienced by the solar cell per unit wavelength (given by the ASTM AM1.5 solar spectrum [2]), $A(\lambda)$ is the absorption calculated above, E_g is the band gap energy, kT is the thermal energy at the operating temperature T, n is the average refractive index of the semiconductor, and the $n^2 + 1$ prefactor is derived by assuming an absorbing semiconductor substrate (as in Ref. 39). Next, the open circuit voltage is calculated by setting $J = 0$. Finally, the fill factor is found by setting the derivative $d(JV)/dV = 0$ and solving for $V(\max)$ and $J[V(\max)]$.

In order to understand the basic properties of the photonic crystal lattices used in this paper, the eigenmodes of Maxwell's equations with periodic boundary conditions, also known as a photonic bandstructure, are computed by preconditioned conjugate-gradient minimization of the block Rayleigh quotient in a planewave basis, using a freely available software package [40].

3. Results and discussion
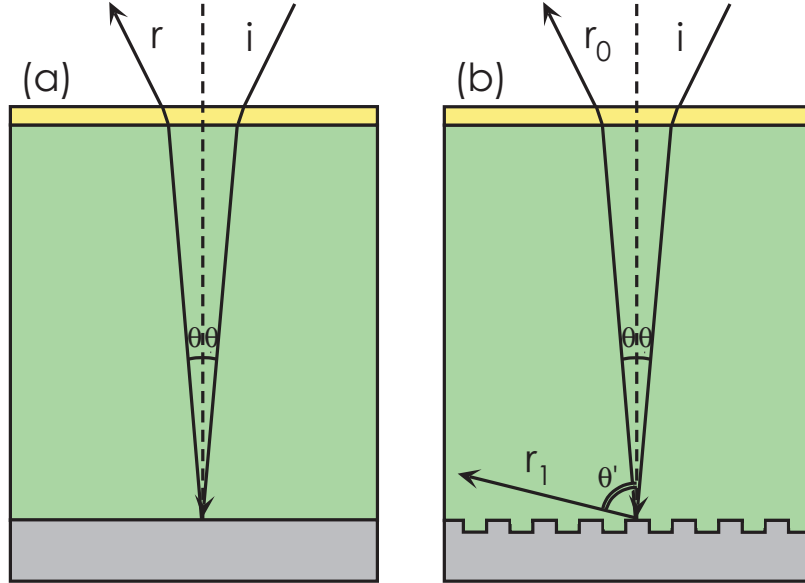
3.1. Metallic designs

Fig. 2. Illustration of two metallic solar cell designs: (a) a common design with a perfect metal backing and no front surface texturing, which displays only spectral reflection; (b) a metal with periodic grating on the back [21–25]. Crystalline silicon is in green, metal in grey, and air is transparent.

Consider the performance of several metal-based c-Si solar cell designs without surface texturing, which all have a thickness $d = 2\,\mu\mathrm{m}$, for TE-polarized light incident from directly overhead. The first solar cell design consists of an anti-reflection coating made of a transparent dielectric on top of a slab of c-Si (with a substrate also made of c-Si). However, since light can easily escape from the bottom, this design is not commonly used. The more commonly used second design, shown in Fig. 2(a), addresses this problem by using the previous design plus a perfect metallic reflector to force light to pass through the c-Si twice, thus greatly improving the efficiency of thin film c-Si cells. The spectrally reflected mode created by this design is denoted by r. The third design, shown in Fig. 2(b), uses a perfect metallic reflector with a grating optimized for light trapping [21–25]. Spectrally reflected modes are denoted by r_o, while diffracted modes are denoted by r_1, r_2, etc.
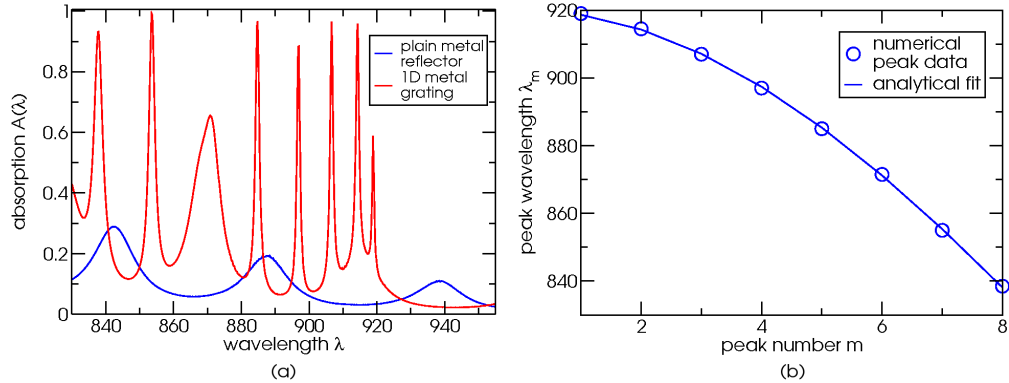

Fig. 3. (a) Absorption versus wavelength for a plain $2\,\mu\mathrm{m}$ c-Si thin film with a perfect metal back reflector, compared to the same structure with a metal grating of period $p = 255$ nm and etch depth 67 nm (b) Absorption peak wavelength as a function of peak number – note that peak spacing increases with peak number, implying diffraction is strongest right at the diffraction threshold (here, 920 nm).

First, consider the optimization of the anti-reflection coating. It is well-known that perfect transmission between two semi-infinite dielectric media may be achieved by choosing a refractive index that is the geometric mean of the indices of the two media, and a thickness that is a quarter of an optical wavelength. Physically, this is possible because the front and back of the AR coating both cause reflections: when the thickness is a quarter of an optical wavelength, it yields a relative phase difference of π, corresponding to destructive interference which cancels reflections [41]. In order for the reflections to be the same amplitude, one must choose the index of the AR coating correctly. For silicon-based solar cells (where $n \approx 3.5$ in the near-IR), silicon nitride ($n \approx 1.91$) is commonly employed, since its index roughly corresponds to the geometric mean of the refractive indices of silicon and air [5]. With a refractive index of 1.91, and a target wavelength of 535 nm, we obtain an optimal thickness of 70 nm, which has been confirmed by simulations. With this optimized AR coating, and no back reflector, the power conversion efficiency is found to be 9.07%. With a perfect metal back reflector, the efficiency goes up to 13.77%.

Further improvement of the efficiency requires adding a means of coupling light into oblique angles. As mentioned previously, past approaches have used surface texturing, but we examine the effect of a grating instead. It must be optimized for the maximum effect, which requires further insight into the physics underlying its operation. The absorption spectrum for a 1D grating is depicted in Fig. 3(a), and compared to that of a planar reflector. One can construct a simple analytical model to explain the diffractive light-trapping mechanism. If a bulk region of

thickness d is considered, then all resonances should pick up a round-trip phase change which is a multiple of 2π, which gives us the condition $k_\perp = \pi m/d$, where m is an integer, and the wavelength of the diffracted mode is given by $\lambda = 2\pi n / \left[G^2 + (\pi m/d)^2 \right]^{1/2}$, where $G = 2\pi l/p$ is a reciprocal lattice vector of the grating, l is the diffraction order, and p is the grating period. Near the diffraction limit, this model predicts that the peak spacing will increase with peak number, and thus, the greatest benefit from diffraction will occur right near the diffraction limit. The comparison in Fig. 3(b) between this simple analytical model for the mode spacings and the numerical data shows excellent agreement. Also, note that if the only source of loss is the material, then the quality factor is given by $Q = n/2k$. This suggests that absorption peaks will be
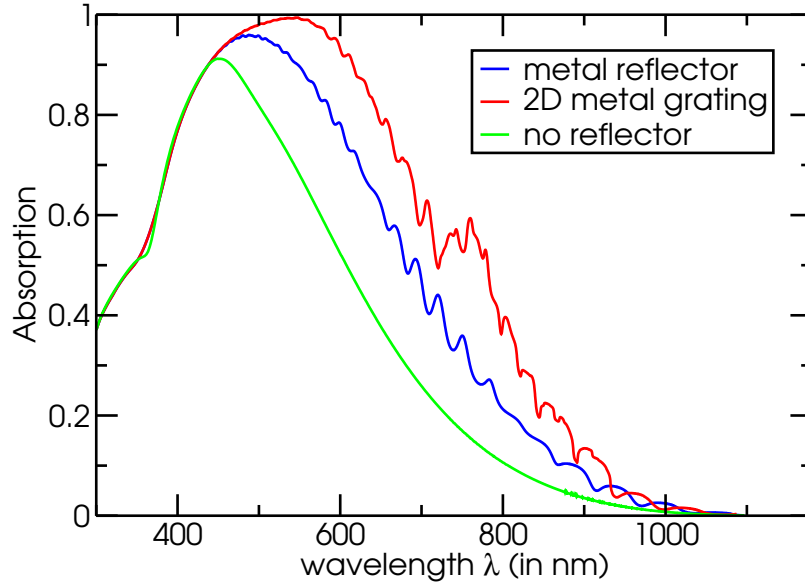
shown

Fig. 4. Absorption vs. wavelength for three 2 μm-thick Si cell designs: no back reflector, perfect metal back reflector (Fig. 2(a)), and perfect metal grating with a 2D-periodic "checkerboard" pattern of period 255 nm in both lateral directions and an etch depth of 67 nm (Fig. 2(b)). Note that the narrow peaks seen in Fig. 3 are smoothed out with a moving average that preserves the area under the curve.

In numerical optimization of the grating, the first parameter that must be determined is the period of the grating p. Following previous work (e.g., Refs. 14, 16, and 22–24), it is chosen so that first order diffraction (i.e., $l = 1$) will occur in the near-IR. Through simulations, its value is determined to be 255 nm, corresponding to a diffraction threshold of 920 nm in c-Si. In either case, the exact optimal periodicity will depend slightly on the thickness of the active region, and will be shifted to longer wavelengths for thicker cells (since they will already be absorbing shorter wavelengths well), as observed in Ref. 14. One could alternatively use a second order diffraction grating instead (i.e., $l = 2$), as in Ref. 25; Ref. 16 finds about a 1-2% improvement in using a second-order grating for a particular set of parameters. Overall, it is found that the performance of the second order gratings is similar to first order gratings for our choice of periodicity. This is consistent with the findings of Ref. 14.

Furthermore, there are a variety of other parameters to be considered, such as profile shape, incident angle and polarization, profile, duty cycle, and etch depth [26]. The rectangular

(square-wave) profile is chosen because it is a simple structure that has been shown to perform better than a symmetric triangular pattern [26]. The duty cycle f, i.e., the fraction of dielectric that is raised over each period, is chosen to be exactly one-half for the reason that the largest Fourier components responsible for diffraction will occur at that value. Ref. 14 provides numerical calculations suggesting that a slight departure from this value can achieve a very small performance enhancement; however, that effect is neglected in this work. This is consistent with the finding of Ref. 16. Finally, consider the etch depth: at its optimal value, specular reflection will be at a minimum (due to destructive interference), thus forcing incoming light to be diffracted into guided modes. However, since the wavelength is comparable to the period and depth of the grating, one cannot use a scalar theory to determine its value. Instead, one can employ the simulation techniques discussed above to show that the best etch depth is 67 nm. In the idealized case that the metal does not absorb any light – a "perfect" metal – the following remarkable results are obtained: for a 1D periodic grating, the efficiency is found to be 17.88% (neglecting recombination losses). Furthermore, one can envision improving upon the 1D gratings by incorporating a second, orthogonal periodicity that is also parallel to the surface of the solar cell, i.e., a 2D grating, which makes a "checkerboard" pattern. For such a grating, the efficiency in the optimal case is found to be 19.29%. The corresponding absorption spectra are shown in Fig. 4. The additional considerations in designing a 2D grating are discussed in the next section.

Results for the perfect metal case should be interpreted with care: it is well-known that a real metal will introduce losses. Consider a plain aluminum back reflector, subject to reflection losses, as quantified in Ref. 42. We have performed simulations that show the efficiency of a solar cell with an aluminum back reflector is decreased by 8.2% relative to a perfect metal, to an absolute efficiency of 12.72% (again, neglecting recombination losses). Using a metal grating will also introduce surface plasmon losses, which means that the actual efficiencies will be degraded by more than 8.2%, relative to the perfect metal grating. Evaluating the magnitude of the surface plasmon loss goes beyond the scope of this paper. Nonetheless, the point remains that metal grating structures will not see nearly as dramatic of an efficiency improvement as one might initially expect. This result has driven recent interest in all-dielectric structures.

3.2. Dielectric designs

3.2.1. DBR-based designs

Now consider the performance of three dielectric-based solar cell structures based on a 2 μm thin film of c-Si. The first design, shown in Fig. 5(a), consists of an anti-reflection coating on top and a distributed Bragg reflector (DBR) in the bottom. In creating a DBR design that reflects strongly in the near-IR, the materials are chosen to be c-Si ($n \approx 3.5$) and SiO_2 ($n = 1.5$) because they represent a low cost and readily available method of making a reflector with a large bandwidth, which was considered in Refs. 13–16. Given the target wavelength range and materials, a period $a = 150$ nm is chosen. Using 10 bilayers of c-Si and SiO_2 yields high reflectivity (over 99%) over most of the critical wavelengths that are difficult to absorb in silicon. The overall efficiency is found to be 12.44%, which compares well to the aluminum reflector efficiency of 12.72%. The slightly greater losses of a cell with a DBR reflector compared to an aluminum reflector comes about because the limited bandwidth of the reflectors has a slightly greater effect than the Ohmic losses of the aluminum. Thus, the DBR will be used as a benchmark for evaluating the relative efficiency improvements of the subsequent dielectric structures. Note that similar efficiencies are also seen for a flat aluminum reflector.

The second dielectric design, shown in Fig. 5(b), based on the one studied in Refs. 13–16 consists of an anti-reflection coating, a DBR on the bottom, and a periodic grating in the back of the top low-index SiO_2 layer of the DBR. It should be noted that the introduction of the grating
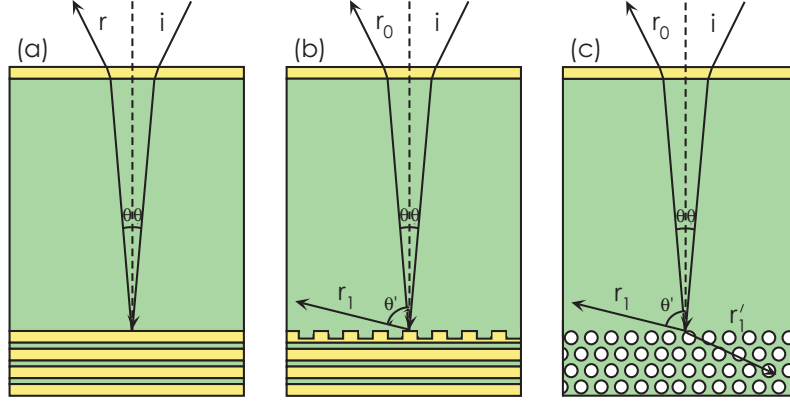
Fig. 5. Illustration of three solar cell designs: (a) a simple design with a distributed Bragg reflector (DBR), which displays only spectral reflection [13–16] (b) a DBR plus a periodically etched grating, displaying spectral reflection and diffraction [13–16], and (c) a photonic crystal consisting of a triangular lattice of air holes, displaying simultaneous reflection, diffraction, and refraction from the photonic crystal layer (based on Ref. 6). Crystalline silicon is in green, low dielectric in yellow, and air is transparent.

into the omnidirectional reflector can, in principle, cause coupling into propagating modes in the reflector, thus eliminating perfect omnidirectional reflectivity.

The results for c-Si wafers with thicknesses varying from 2 μm to 32 μm, and backed with a DBR ($a = 165$) etched with a 1D grating with period 310 nm and etch depth 67 nm are shown in Fig. 6 (after smoothing over the narrow peaks seen in Fig. 3 in a way that preserves the area under the curve). In analyzing these results, it is observed that overall absorption goes up with thickness, as expected, due to the greater number of modes supported by the bulk semiconductor region. However, the relative enhancement of light trapping is greater for thinner films, because they have lower baseline absorption. For a 2 μm-thick c-Si film, the greatest absorption enhancement of about a factor of five occurs around a wavelength of 1060 nm. This result is consistent with the observation that the density of peaks is greatest near the diffraction limit, as illustrated in Fig. 3.

However, when we optimize the parameters for a 2 μm-thick sample of c-Si, we find that the parameters are similar but not identical to those of a metallic structure of equal thickness, specifically, for a DBR ($a = 165$ nm) with an etching period of 264 nm, and etch depth of 67 nm. The efficiency as a function of the number of bilayers is given in Table 1; for the particular case of 8 DBR bilayers, an efficiency improvement from 12.44% to 15.42% is observed.

Now, consider the problem of creating a 2D grating in the DBR structure. An interesting but non-trivial question is how to choose the second period. If the first period is denoted by p_x, and the second by p_y, one might naïvely set $p_y = p_x$; however, this creates two strongly overlapping sets of diffraction modes. Thus, the optimal design will have $p_y \neq p_x$. Furthermore, as p_x increases, p_y and p_y/p_x should both decrease in order to ensure both grating directions contribute to light trapping within the optimal wavelength range for a given thickness of c-Si. In Fig. 7, three different values of p_x ranging from 330-417 nm are used: as predicted, the smallest value of $p_x = 330$ nm yields a peak at $p_y/p_x = 1.3$, while the largest value of $p_x = 417$ nm yields a peak around $p_y/p_x = 0.85$. Also, as would be expected, 2D gratings with optimized grating parameters perform better than 1D gratings. While a 1D grating with 4 bilayers and $p_x = 374$ nm has an efficiency of 15.37%, a 2D grating with $p_x = 374$ nm and $p_y = 411$ nm with 4 bilayers has an efficiency is 16.27% (5.6% higher). Further results are given in Table 1. Also,
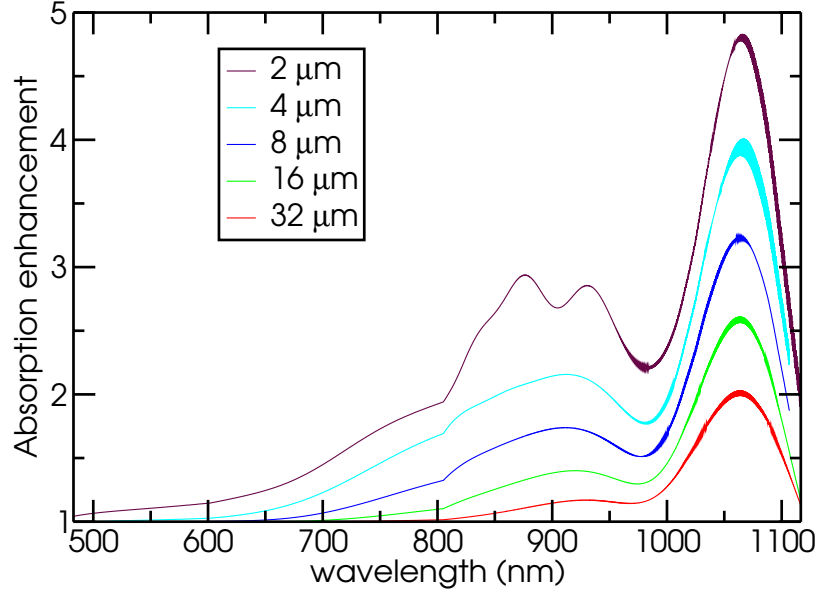
Fig. 6. Illustration of the enhancement of the absorption spectrum created when introducing a 1D grating into a DBR ($a = 165$) with period 310 nm and etch depth 67 nm, quantified as the quotient of the absorption with the grating with the absorption without it. Note that the narrow peaks seen in Fig. 3 are smoothed out with a moving average that preserves the area under the curve.

Table 1. Percentage efficiency of various solar cell designs as a function of the number of periods in the z-direction for a plain distributed Bragg reflector (DBR), a DBR with 1D and 2D etched gratings (based on Fig. 5(b)), a triangular photonic crystal of air holes in silicon (based on Fig 5(c)), a woodpile of air trenches in silicon (based on Ref. 43), and an inverse silicon opal (based on Ref. 44).

# periods	1	2	3	4	5	6	7	8
DBR	10.69	11.99	12.35	12.42	12.44	12.43	12.42	12.44
DBR + 1D grating	12.11	14.47	15.21	15.37	15.41	15.41	15.42	15.42
DBR + 2D grating	12.50	15.29	16.09	16.27	16.30	16.32	16.32	16.32
triangular PhC	13.99	15.01	15.26	15.49	15.59	15.70	15.74	15.79
woodpile PhC	13.43	14.20	14.69	14.92	15.07	15.19	15.35	15.42
inverse opal PhC	12.82	13.77	14.38	14.79	15.09	15.35	15.59	15.73

note that there may be better 2D grating patterns than the checkerboard pattern investigated in this manuscript; for instance, Ref. 21 suggests a triangular lattice.

One shortcoming of the DBR plus grating design is that some incoming beams may propagate through the DBR, thus exiting the cell without being absorbed. The reason is two-fold: first, the DBR examined here and in previous work [13, 15, 16] is not an omnidirectional reflector for light coming from a high index medium such as silicon. Furthermore, even if it was, the grating breaks the symmetry in the transverse direction, which means transverse momentum is not conserved, so incoming light with a frequency above the diffraction threshold could couple to propagating modes inside the DBR. The only way to avoid this shortcoming is to use a photonic crystal displaying a true band gap for all directions in which light can be diffracted (this
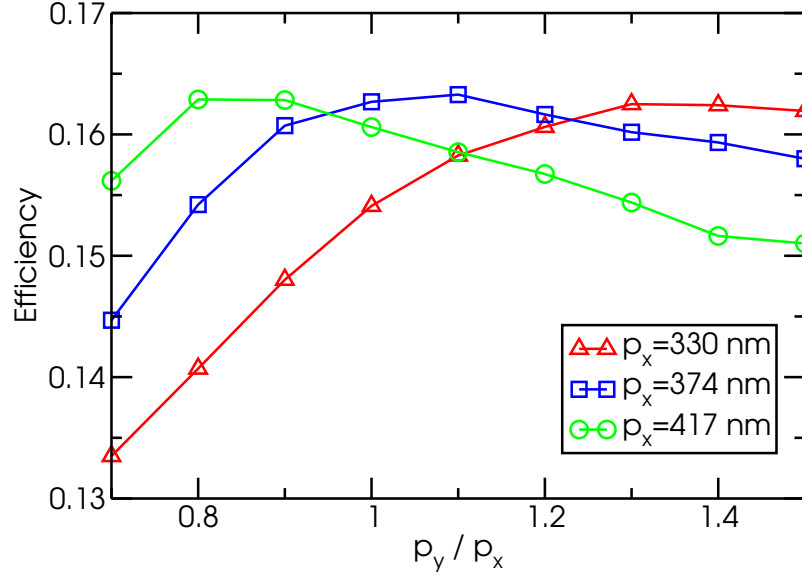
Fig. 7. Efficiency of power generation versus p_y/p_x for the geometry described in the text: a 4-bilayer DBR with a 2D "checkerboard" pattern etch ($t = 2\,\mu$m, $a = 165$ nm, $e = 67$ nm). Three different values of p_x are used; as predicted, smaller values of p_x see peak efficiencies at higher values of p_y/p_x.

will vary depending on the design).

3.2.2. Photonic crystal-based designs

The third design, illustrated in Fig. 5(c), consists of an anti-reflection coating in the front, and a photonic crystal in the back, made of a 2D triangular lattice of air holes, with an air hole radius of $r = 0.375a$, where a is the lattice periodicity. Aside from the diffracted modes, which are labeled in the same fashion as those in the grating, additional modes which penetrate into the photonic crystal before reflection or loss out the backside are denoted along the path r_1'. Thus, this design effectively has more silicon that can be used for absorption (since it is not surrounded by dielectric). On an experimental note, electron-hole recombination could be prevented through oxidation of the air-silicon interfaces, which would create a thin layer of silica for passivation. It would also be possible to use hydrogen gas for passivation, or to fill the holes entirely with a passivating material.

A similar structure with a square lattice of air holes was envisioned in Ref. 6, but to the best of our knowledge, has not been studied in detail any further since then, either theoretically or experimentally, until now. The reason why we choose to use a triangular lattice can best be understood by referring to the bandstructures for each design. First let us note that the bandstructure and some absorption spectra are computed in reduced frequency units ω in multiples of $2\pi c/a$, rather than physical wavelength λ in nm; the conversion is given by $\lambda = a/\omega$, where a is the period of the photonic crystal in nm. The results are presented in this way because the scale invariance of Maxwell's equations ensures that the results will be true for any a [31]. Now compare the bandstructure of a square lattice of air holes, based on Ref. 6, as shown in Fig. 8(a), to the bandstructure for a triangular lattice of air holes shown in Fig. 8(b). The triangular lattice offers a large gap of 48% for TE-polarized light, instead of the modest 9.7% TE bandgap of the square lattice: this comes about from the more circular first Brillouin zone. Note that no real

gap is observed for TM-polarized light for either structure, here. As a result of the larger TE gap, the bands surrounding it become flatter, which also enhances light trapping. The reason is that flat bands imply slow group velocities, which means that light will spend more time inside the photonic crystal. Note that it is possible to simultaneously create a gap for TE and TM polarized light with a triangular lattice, but the overall light-trapping performance is found to be worse, since such a structure has a much smaller TE gap.
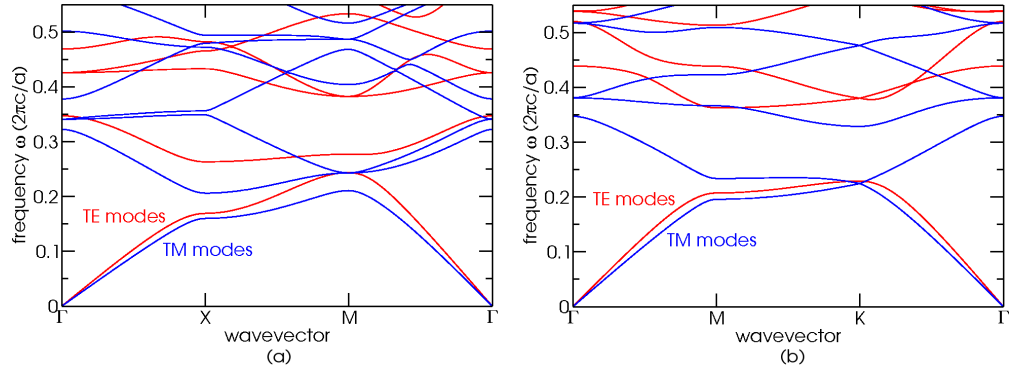

Fig. 8. Bandstructures of two photonic crystal structures made of circular air holes in a high index medium ($n = 3.5$) and radius $r = 0.375a$, arranged in (a) a square lattice and (b) a triangular lattice. Note that the triangular lattice provides a larger gap between TE modes, which also results in flatter bands.

Subsequently, we optimized the design for a 2 μm-thick sample of c-Si, and in that process, proved that a triangular lattice offers performance superior to the square hole structure. The optimal lattice periodicity a is found to be 305 nm. The air holes in the bulk have radius $r = 114$ nm, while the front layer has a slightly flattened, nearly rectangular structure with a fill factor of 0.5 and a thickness of 145 nm, in order to enhance diffraction. The efficiency as a function of the number of rows for the optimized structure are given in Table 1. The most comparable structure, consisting of a DBR plus a 1D grating, has a slightly lower efficiency than the 2D triangular photonic crystal lattice, regardless of the number of periods. That is because while both systems offer similar degrees of reflection and refraction, there are two small additional effect specific to a 2D or 3D photonic crystal made of the photovoltaic material, as mentioned previously. First, this photonic crystal will reflect light incident from air at any angle for TE polarization over a range of frequencies, as well as TE light diffracted by the photonic crystal (in contrast with a DBR plus grating system). Additionally, frequencies outside the photonic band gap are refracted into modes with a high photon density of states [12]. This also explains why the absorption efficiency continues to increase with the thickness of the photonic crystal, while the efficiency of the DBR plus 1D grating system plateaus after 5 bilayers.

The absorption spectra at normal incidence of four different 2 μm-thick c-Si solar cells are shown in Fig. 9. Note that the narrow peaks seen in Fig. 3 are smoothed out with a moving average that preserves the area under the curve. The designs and their overall power generation efficiencies are as follows: a simple anti-reflection coating (no back reflector), with an overall efficiency of 9.07%; an AR coating plus 6 bilayers of DBR, with an overall efficiency of 12.43%; an AR coating plus 6 bilayers of DBR with optimized 1D etching, with an overall efficiency of 15.41% (24.0% higher than the plain DBR); and finally, an AR coating plus 6 layers of photonic crystal air holes in a triangular lattice, with an overall efficiency of 15.70% (26.3% higher than the plain DBR). The photonic crystal design offers the best performance overall, due to two factors: first, the grating causes a small amount of light to be scattered into
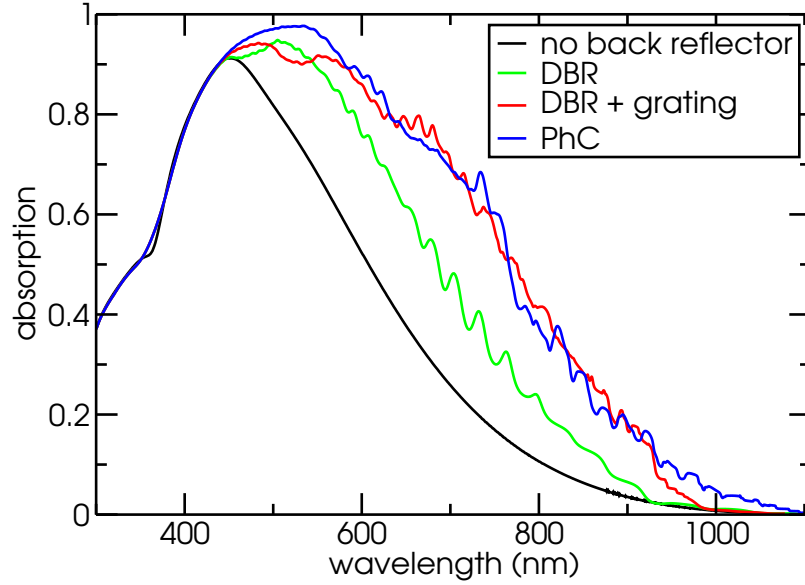
Fig. 9. Absorption vs. wavelength at normal incidence for four 2 μm-thick Si cell designs with continuous symmetry in at least one dimension: no back reflector, plain DBR, DBR plus 1D-periodic grating, and finally, a 2D photonic crystal of air holes in silicon. The last two designs consist of six complete layers. The DBR plus grating and the photonic crystal-based design yield the highest efficiencies, and have very similar magnitudes.

modes that are no longer reflected by the DBR, and the photonic crystal provides an extra region of silicon to absorb light – in the DBR design, the c-Si regions making up the reflector are electrically isolated and cannot contribute to current generation.

Now let us consider some realistic, optimized 3D photonic crystal-based designs. For a 6 bilayer DBR with a period of 165 nm having a 2D grating etched 67 nm deep with periods of 338 nm and 406 nm, we found an efficiency of 16.32% (31.3% above the plain DBR design), as shown in Table 1. Also, for an inverse fcc lattice of silicon with eight layers of air spheres, as made in Ref. 44, with a period of 750 nm and a radius of 262 nm, we found the efficiency to be 15.73% (26.5% above the plain DBR design). Finally, for a woodpile structure [43] made by drilling trenches of air into silicon, 8 periods deep, similar to Ref. 45, with a period of 460 nm and an air filling fraction of 72%, the efficiency is 15.42% (24.1% above the plain DBR design), as shown in Table 1. Here, due to the limited number of design parameters for the uniform photonic crystals, the DBR plus 2D grating shows the greatest efficiency enhancements. However, note from the data in Table 1 that a larger number of periods, if possible to fabricate experimentally, can provide even a slightly greater boost in efficiency; also, a smaller number of periods, which have already been made experimentally (as in Ref. 45) can still offer a significant efficiency boost.

4. Conclusion

In conclusion, two approaches to enhancing solar cell efficiencies through light trapping have been studied: geometrical optics and wave optics. It is found that wave optics can vastly outperform geometrical optics within the range of wavelengths (roughly 700-1100 nm) requiring enhancement in thin films of c-Si. These approaches enhance absorption up to nearly a factor of five at certain wavelengths for a 2 μm-thick film (somewhat less for thicker films). Fur-

thermore, the overall efficiency of such a cell is increased 24.0% by adding an optimized 1D grating to a 6 bilayer DBR; 31.3% by adding an optimized 2D grating; 26.3% by replacing the DBR and grating with a six-period 2D triangular photonic crystal made of air holes in silicon; and 26.5% by replacing the triangular photonic crystal with an eight-period 3D inverse opal photonic crystal, made of air holes arranged in an fcc lattice in c-Si. Based on these results, the two mechanisms of reflection and diffraction shared by the DBR plus grating, as well as the photonic crystal, make the most important contribution to the efficiency of the cells. Photonic crystals made of the photovoltaic material potentially offer slightly higher performances, due to their ability to generate additional photocarriers through refraction into outside of the photonic band gap. However, further work is needed on more complex 3D photonic crystal designs before the maximum contribution of this advantage can be quantified.